Spin crossover complexes [Fe(NH2trz)3](X)2*nH2O investigated by means of polarized Raman scattering and DFT calculations.

Yeny A Tobon, Lara Kabalan, Sébastien Bonhommeau, Nathalie Daro, Arnaud Grosjean, Philippe Guionneau, Samir Matar, Jean-François Létard, François Guillaume

Spin crossover complexes $[Fe(NH_2trz)_3](X)_2 \cdot nH_2O$ investigated by means of polarized Raman scattering and DFT calculations†

Yeny A. Tobon,[ab] Lara Kabalan,[c] Sébastien Bonhommeau,[a] Nathalie Daro,[c] Arnaud Grosjean,[c] Philippe Guionneau,[c] Samir Matar,[c] Jean-François Létard[c] and François Guillaume*[a]

Vibrational spectra of the spin crossover (SCO) polymers $[Fe(NH_2trz)_3](X)_2\ nH_2O$ where NH_2trz = 4 NH_2 1,2,4 triazole and X = Cl, Br, BF_4, and NO_3 have been analyzed. Our results show that the anions and water molecules have no significant influence on the vibrational properties of the $Fe(NH_2\ trz)_3$ polymer chains. A detailed study of the nitrate derivative, based on the DFT analysis of the polarized spectra of single crystals, has been undertaken to propose the normal mode assignment of the Raman peaks in the low spin state of the compound. Changes in the Raman spectra in the high spin state could therefore be analyzed and interpreted by several Raman bands identified as molecular probes of the SCO phenomenon. Various factors (laser power, humidity, pressure) that influence the transition temperatures and the hysteresis loops have been identified and adjusted for obtaining reliable measurements. We demonstrate in particular that all the techniques used to probe the phase transition process give comparable results providing that the sample environment is well controlled.

Introduction

Transition metal complexes in which the spin state of the metal changes under external stimuli such as temperature, light irradiation or pressure have been extensively studied in the past few decades due to their high relevance for potential applications in information processing, sensors and/or display devices,[1–3] and even more recently in the photovoltaic domain.[4] The spin crossover (SCO) phenomenon is a transition from a low-spin (LS) ground state electron configuration to a high-spin (HS) metastable state of the metal d atomic orbitals. Future applications of SCO materials in information storage and optical switching would require a spin transition that is fast (*i.e.* in the picosecond or femtosecond timescale), with a large thermal hysteresis centered at room temperature. Thus, the spin transition process must be highly cooperative and such a requirement is met in polymeric spin-transition compounds.[3,5–8] Some of the most promising polymeric SCO compounds are formed with the triazole ligands threefold bridging the Fe(II) metal ions (Fig. 1). Moreover, light-induced phase transitions occur in these materials opening very promising ways for designing new optical storage devices.[9,10] Within this family of SCO compounds, $[Fe(NH_2\text{-}trz)_3](X)_2$ (with NH_2-trz = 4-amino-1,2,4-triazole and X is an anion) has been investigated quite extensively over the last few years.[9,11–16] These compounds in the

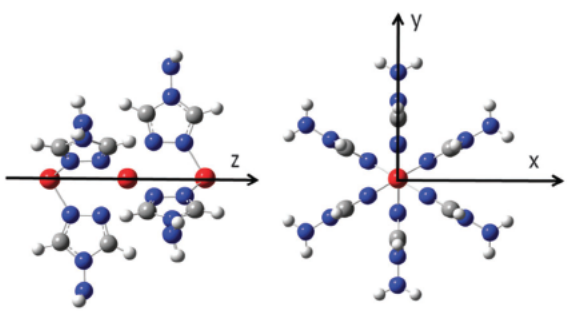

Fig. 1 Representation of the model system $[Fe_3(NH_2\ trz)_6]^{6+}$ of SCO compounds formed with triazole ligands and its reference frame for the DFT calculations. The C_3 symmetry axis is collinear to the *z* axis and the origin is located on the central Fe atom (red ball), according to the standard convention for the point group symmetry D_{3d} operations. Blue, grey and white balls represent N, C and H atoms.

[a] *Université Bordeaux 1, CNRS UMR 5255, ISM, 351 cours de la Libération, 33405 Talence Cedex, France. E mail: f.guillaume@ism.u bordeaux1.fr*
[b] *Université de Lille 1, CNRS UMR 8516, LASIR, Bât. C5, 59655 Villeneuve d'Ascq Cedex, France. E mail: Yeny.Tobon Correa@univ lille1.fr*
[c] *CNRS, Univ. Bordeaux, ICMCB, UPR 9048, 87 avenue du Dr A. Schweitzer, F 33608 Pessac, France. E mail: letard@icmcb bordeaux.cnrs.fr*

LS state as well as in the HS state form linear chains of Fe(II) ions bridged by three NH_2-trz molecules. The LS–HS transition is always accompanied by an increase in the crystal volume corresponding to about 1 to 5% in most cases due to the large modifications in the coordination environment of the transition metal.[3] This increase is notably important for the polymeric SCO compounds of general formula $[Fe(R\text{-}trz)_3](X)_2$. In the latter indeed, the magnitude of the crystal volume expansion at the SCO is about twice that of the one encountered in discrete molecular SCO compounds, reaching 10% at the maximum observed so far.[17] Significant effects are thus expected on the vibrational properties of the crystal and of the ligands. Vibrational Raman spectroscopy is a well-recognized technique to characterize the phase transition process in SCO compounds.[18–21] It is usually preferred to infrared (IR) spectroscopy because raw samples in small amounts ($\sim\mu g$) can be directly analyzed, while Fourier Transform IR (FTIR) techniques often involve the preparation of large pellets composed of SCO and KBr powders, which is prone to affect the SCO phenomenon due to the internal pressure exerted on the SCO molecules. It is also better adapted than IR spectroscopy to scrutinize vibrations with wavenumbers ranging below 600 cm^{-1}.

Because of the complexity of these systems, the interpretation of SCO vibrational spectra is still a difficult task. Density functional theory (DFT) calculations on spin crossover systems have appeared only recently.[21–23] The combination of vibrational spectroscopy and quantum chemical calculations should help significantly in the assignment of the observed bands, providing therefore a better understanding of the relationships between the molecular properties and the observed macroscopic effects. Very few comprehensive studies on the vibrational properties of SCO systems have been published in the literature so far. In some studies the wavenumbers calculated by means of DFT methods were compared to values inferred from IR or Raman experiments for powder specimens.[15,24–29] In general the emphasis was put on interpreting the experimental spectra at wavenumbers below 600 cm^{-1} where the external vibrations involving the Fe–ligand bonds are expected. Ideally the theoretical DFT calculations should be performed using periodic boundary conditions (PBC-DFT) and the Raman scattering experiments should be carried out on oriented single crystals. Thus polarization effects in Raman spectroscopy could be exploited to assign the observed spectral features. However, the calculation of vibrational spectra by means of PBC-DFT methods remains certainly a very complex task for SCO polymers (only two papers[30,31] have reported such calculations but no vibrational analysis was described there) and, to the best of our knowledge, Raman spectra of oriented single crystals have never been recorded or published so far.

We will show that polarized Raman experiments performed on single crystals of an SCO compound help significantly in the interpretation of the vibrational spectra of SCO polymers. Among these SCO coordination polymers, the nitrate derivative of the SCO $[Fe(NH_2\text{-}trz)_3]$ polymer displays the widest thermal hysteresis loop centered at room temperature. In addition, $[Fe(NH_2\text{-}trz)_3](NO_3)_2{\cdot}2H_2O$ single crystals have been recently synthesized,[16] offering for the very first time the opportunity to perform a detailed analysis thanks to polarized Raman spectroscopy measurements on this family of SCO compounds.

The temperature dependence of vibrations below 600 cm^{-1} was described qualitatively by means of Raman spectroscopy in the SCO $[Fe(NH_2\text{-}trz)_3](ClO_4)_2$ compound by E. Smit *et al.*[14] Very recently, the vibrational properties of SCO $[Fe(NH_2\text{-}trz)_3](X)_2$ compounds with X = Cl, CH_3SO_3 and $C_{10}H_7SO_3$ were investigated, only below 600 cm^{-1}, by means of nuclear inelastic scattering, Raman spectroscopy and DFT calculations by S. Rackwitz *et al.*[15] However, a thorough vibrational assignment of Raman active modes of SCO $[Fe(NH_2\text{-}trz)_3](X)_2$ compounds is still missing. The first goal of this paper is therefore to propose a full vibrational assignment by combining Raman scattering and DFT calculations. As $[Fe(NH_2\text{-}trz)_3](NO_3)_2{\cdot}2H_2O$ single crystals are now available, we will focus mainly on this specific compound and develop successively four items related to it. In the first one, we will analyze the influence of counterions and water molecules on the vibrational properties of the family of complexes $[Fe(NH_2\text{-}trz)_3](X)_2{\cdot}nH_2O$ with X = Cl, Br, BF_4, NO_3 in both LS and HS states. In the second subsection, we will compare the experimental and theoretical polarized Raman spectra of the complex $[Fe(NH_2\text{-}trz)_3](NO_3)_2{\cdot}2H_2O$ in its LS state (298 K) to propose an assignment of the observed modes. In the third subsection, we will interpret the structural modifications induced by the transition between the LS and HS states and finally, in the last subsection, we will compare the measured hysteresis loops of $[Fe(NH_2\text{-}trz)_3](NO_3)_2{\cdot}H_2O$ inferred from the thermal evolution of a specific spin-state-dependent Raman spectral region to those obtained by means of other macroscopic techniques.

Methods

The preparation of the $[Fe(NH_2\text{-}trz)_3](NO_3)_2{\cdot}H_2O$ was obtained as described in the literature[32–34] from the mixture of $FeSO_4{\cdot}7H_2O$ and $Ba(NO_3)_2$ in water to firstly prepare the $Fe(NO_3)_2$ salt, and then by adding the 4-amino-1,2,4-triazole (NH_2-trz) ligand. The elemental analysis performed on the powder of the nitrate complex is consistent with the presence of one molecule of water in the structure with formula $[Fe(NH_2\text{-}trz)_3](NO_3)_2{\cdot}H_2O$. Micrometric needle-shaped single crystals of $[Fe(NH_2\text{-}trz)_3](NO_3)_2{\cdot}2H_2O$ were obtained by the slow diffusion method.[16]

The Raman spectra were recorded in the backscattering geometry with a Labram HR 800 Raman spectrometer (Horiba Jobin-Yvon) coupled to an Olympus confocal microscope and equipped with a laser operating at 514.5 nm. The powder samples of $[Fe(NH_2\text{-}trz)_3](NO_3)_2{\cdot}H_2O$ were placed in a Linkam stage allowing the control of the temperature (between 25 °C and 120 °C in these experiments), the pressure (between 1 and atmospheric pressure 101.3 kPa) and the environment (air, dry nitrogen) conditions. The experiments in the LS state were performed at 25 °C and those in the HS state were performed at 100 °C. To avoid excessive heating of the powder sample due to the laser irradiation, we used the DuoScan™ accessory (Horiba Jobin-Yvon) based on a combination of scanning mirrors that ensure a uniform scanning of the laser beam over an area of about 400 μm^2. In addition, for the hysteresis loop measurements the

laser power on the sample surface was kept below 8 μW. The experiments on isolated particles or single crystals were performed at room temperature (25 °C). In general, a 50× Olympus objective was used in the Raman experiments, except for those performed on single crystals of $[Fe(NH_2\text{-}trz)_3](NO_3)_2{\cdot}2H_2O$ that must be kept in water to avoid damage (a water immersion 60× objective was used). The average spectral width of the instrumental resolution was about 6 cm^{-1} (FWHM) and the calibration of the instrument was performed using a silicon standard before each experiment.

The quantum chemical calculations were performed using the Gaussian 09 software.[35] DFT hybrid functional B3LYP was employed in combination with a 6-31+G* basis set for the C, H and N atoms, and LANL2DZ[36] including an effective core potential for Fe atoms[37] which incorporates the mass velocity and Darwin relativistic effects. Geometry optimizations were sought using standard gradient techniques by simultaneous relaxation of all the geometrical parameters. The calculated vibrational properties correspond in all cases to potential energy minima for which no imaginary vibrational frequency was found. As discussed in the next section, no specific scaling was applied to the calculated wavenumbers.

Additional IR spectra of $[Fe(NH_2\text{-}trz)_3](X)_2{\cdot}nH_2O$ powder samples were recorded using a Nexus Nicolet FTIR instrument equipped with an MCTB detector in the range 4000–400 cm^{-1}, with a resolution of 4 cm^{-1}. The sample was placed into a golden gate single reflection diamond ATR accessory at 25 °C in the LS state and at 100 °C in the HS state.

Results and discussion

Influence of counterions and water molecules on the vibrational properties of $[Fe(NH_2\text{-}trz)_3]$

Raman spectra of $[Fe(NH_2\text{-}trz)_3](NO_3)_2{\cdot}H_2O$ in the LS and HS states are displayed in Fig. 2 and 3. According to previous analysis of the vibrations of the NH_2-trz molecule[38,39] (Table S1 in ESI†), N–H and C–H stretching vibrations are observed between 3000 and 3500 cm^{-1}; the bending modes of the amino group NH_2 are active at around 1650 cm^{-1}; and all modes of the triazole ring involving in particular coupled N–N and C–C stretching modes are expected between 600 and 1500 cm^{-1}. Finally a few intramolecular vibrations involving bending and torsion vibrations give rise to low intensity bands in the Raman spectra between 200 and 500 cm^{-1}. A strong Raman peak is also expected at around 1050 cm^{-1} for the symmetric stretching mode of the nitrate anion. Note that external vibrations involving the overall displacement of the iron atoms and of the ligands are expected[14,15] below 600 cm^{-1}.

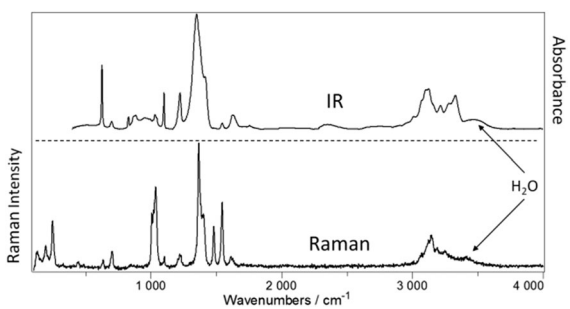

Fig. 2 IR (top) and Raman (bottom) spectra of a powder sample of $[Fe(NH_2\ trz)_3](NO_3)_2{\cdot}H_2O$ at room temperature in the LS state.

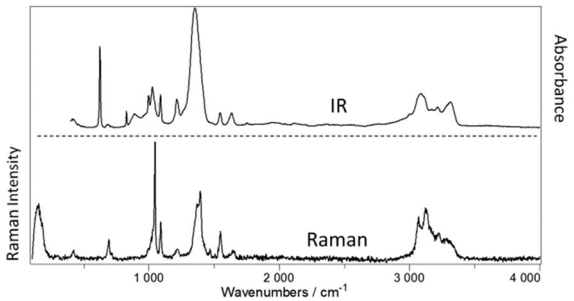

Fig. 3 IR (top) and Raman (bottom) spectra of a powder sample of $[Fe(NH_2\ trz)_3](NO_3)_2{\cdot}H_2O$ at room temperature in the HS state at 373 K.

The Raman and IR spectra of $[Fe(NH_2\text{-}trz)_3](NO_3)_2{\cdot}H_2O$ powder recorded in air at room temperature in the LS state (see Fig. 2) show low intensity bands at around 3500 cm^{-1} that are characteristic of water. These bands disappear upon heating the sample up to ~373 K (see Fig. 3) in the HS state and reappear upon cooling down to room temperature. If the sample is cooled down to room temperature in an atmosphere of dry nitrogen, the bands due to water do not reappear but all the other bands belonging to the ligands or the anionic species remain unchanged compared to the hydrated compound. Thus, the presence of water in the sample has no significant influence on the vibrational properties of the $Fe(NH_2\text{-}trz)_3$ polymer chain. Furthermore, we have recorded the Raman spectra in both LS and HS states for several members of the $[Fe(NH_2\text{-}trz)_3](X)_2{\cdot}nH_2O$ family with X = NO_3, BF_4, Br and Cl. Clearly all these spectra (shown in Fig. 4) display nearly identical features (except for bands easily assigned to the totally symmetric stretching vibrations of the anions BF_4^- around 750 cm^{-1} and NO_3^- around 1050 cm^{-1}) so that we may conclude that the vibrational properties of the polymer chain are not significantly modified by the presence of counterions. The same conclusion was reached by S. Rackwitz *et al.*[15] for compounds with X = Cl, CH_3SO_3 and $C_{10}H_7SO_3$. In contrast, the hydration degree appears as a key factor that governs the crystal packing. It is indeed clear, from X-ray diffraction patterns (Fig. S2 in ESI†), that the structural properties of $[Fe(NH_2\text{-}trz)_3](NO_3)_2{\cdot}H_2O$ in powder form are completely different from those of the single crystals of $[Fe(NH_2\text{-}trz)_3](NO_3)_2{\cdot}2H_2O$. It is also known[13,40] that, depending upon the nature of the counterions and the hydration degree, HS-to-LS and LS-to-HS thermal transition temperatures may vary from ~180 K to 340 K and the widths of the hysteresis loops may range from a few Kelvin to ~40 K. Considering that, unlike structural properties, vibrational properties are insensitive to the surroundings of the polymer chains in $[Fe(NH_2\text{-}trz)_3](X)_2{\cdot}nH_2O$ materials, one may conclude that the aforementioned thermal transition temperatures and breadth of hysteresis loops are mainly governed by the crystal packing in this family of SCO complexes.

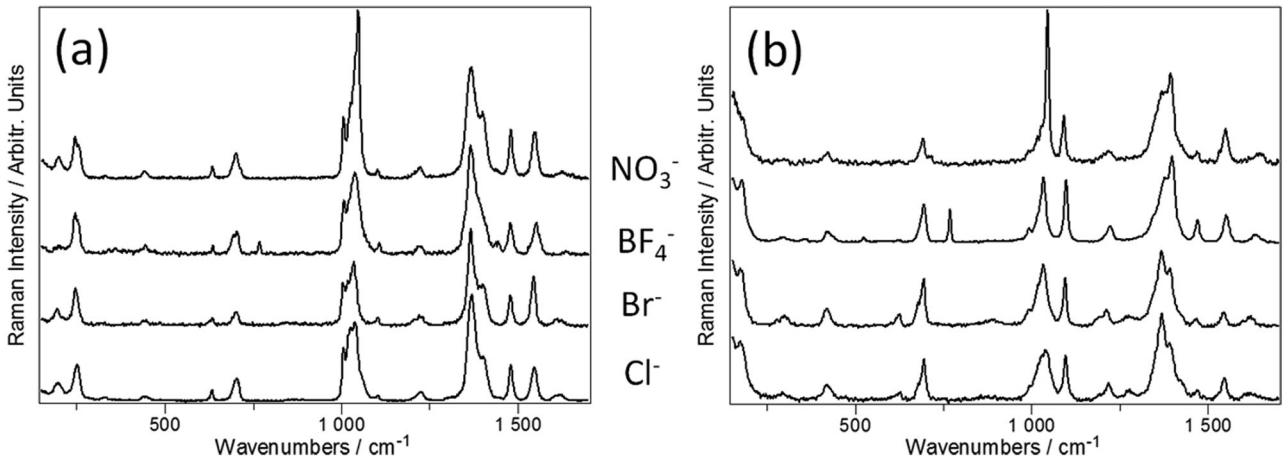

Fig. 4 Raman spectra of the LS (a) and HS (b) states of powder samples of $[Fe(NH_2\ trz)_3](X)_2$ with X = NO_3 , BF_4 , Br and Cl . All spectra were recorded at room temperature in the LS state and at 373 K in the HS state except for the BF_4 derivative for which the spectra were recorded at 173 K in the LS sate and at room temperature in the HS state.

In addition, we have recorded at room temperature and compared with each other Raman spectra of $[Fe(NH_2\text{-}trz)_3](NO_3)_2{\cdot}H_2O$ powder made of particles with different sizes (see above), isolated $[Fe(NH_2\text{-}trz)_3](NO_3)_2{\cdot}H_2O$ powder particles (typical size $5 \times 2\ \mu m^2$) and $[Fe(NH_2\text{-}trz)_3](NO_3)_2{\cdot}2H_2O$ single crystals (needle-like crystal with length $\sim$50 μm and width $\sim$3 μm). For the isolated particles, the Raman spectra remained almost unchanged whatever their orientation with respect to the laser beam polarization direction and were found to be identical to those obtained for the powder. Clearly the complex $[Fe(NH_2\text{-}trz)_3](NO_3)_2{\cdot}H_2O$ does not form single crystals but a crystalline powder. In contrast, Raman bands observed for the single crystals depend on the orientation of the crystals with respect to the polarization direction of the incoming laser beam (see next section). However they fit very well in position and in intensity with bands in the Raman spectra associated with the powder samples and the isolated particles. This result confirms again that the presence of two water molecules for each $[Fe(NH_2\text{-}trz)_3](NO_3)_2$ entity has no significant influence on the vibrational properties of the polymer chain.

Vibrational assignment of Raman bands of $[Fe(NH_2\text{-}trz)_3]$ in the LS state

For $[Fe(NH_2\text{-}trz)_3](NO_3)_2{\cdot}2H_2O$ samples that form needle-like single crystals, Raman spectra were recorded in two different configurations, namely for the long needle axis either parallel or perpendicular to the polarization direction of the incoming laser beam. Defining the laboratory frame with the x axis parallel and the z axis perpendicular to the needle axis, Raman spectra with polarization geometries $y(xx)\bar{y}$, $y(xz)\bar{y}$ and $y(zz)\bar{y}$ (Porto notation[41]) were obtained, where y and $\bar{y}$ denote the direction of the incident laser beam and the outgoing scattered light, respectively, and letters (x or z) in parentheses indicate the corresponding polarization directions. In the following, we will describe the strategy adopted to interpret the experimental Raman spectra of $[Fe(NH_2\text{-}trz)_3](NO_3)_2{\cdot}2H_2O$ in the LS state. Our aim consists in assigning all the observed Raman bands of the polymer chain $[Fe(NH_2\text{-}trz)_3](NO_3)_2$ in the LS state to normal modes with the help of theoretical DFT calculations (see Table 1 for final assignments). In order to illustrate our methodology, special emphasis will be given to the discussion of assignments of Raman peaks in the 150–300 cm^{-1}, 950–1150 cm^{-1} and 1300–1600 cm^{-1} spectral regions.

To construct a theoretical model system, we have considered first, as demonstrated above, that the vibrational properties of the polymer chain are neither significantly modified by counter ion substitution (Fig. 4) nor affected by the presence of water molecules. Second, we have assumed that the FeN_6 octahedron is hardly distorted. Indeed, the crystal structure of $[Fe(NH_2\text{-}trz)_3](NO_3)_2{\cdot}2H_2O$ in the LS state is known[16] to be triclinic with space group $P\bar{1}$, the iron atoms being located on inversion centres, and the FeN_6 coordination sphere being very close to a regular octahedron. Consequently, we have constructed a very simplified model system of the ionic complex $Fe(NH_2\text{-}trz)_3^{2+}$ by considering three Fe atoms and six NH_2-trz ligands, as shown in Fig. 1. The Fe–ligand distances obtained for the optimized structure are 2.1 Å for the central Fe atom and 1.91 Å for the two other Fe atoms. These values compare reasonably well with the experimental ones, namely 1.99 and 1.95 Å determined from X-ray diffraction measurements.[16] Also the Fe–Fe distance of 3.59 Å is in line with the 3.65 Å experimental value[16] (the calculated geometric parameters are listed in Table S3 (ESI†)). We found that most of the calculated wavenumbers for the vibrations of the model system of Fig. 1 are lower than the experimental ones, at least for Raman active modes below *ca.* 2000 cm^{-1}. This downshift in energy is likely due to the unbalanced charges in the model system. It could be reduced upon adding negative charges as shown in the literature.[15] Nevertheless, this correction will not be considered in the current report, because the level of approximation in our model is already sufficient to interpret conveniently Raman spectra.

Table 1 Raman and calculated wavenumbers of the $Fe(NH_2Trz)_3(NO_3)_2$ complex in the low spin (LS) state and proposed assignments

Calculated Raman wavenumbers (cm^{-1}) and symmetry	Experimental wavenumbers (cm^{-1}) in LS state	Assignments[a]	Calculated Raman wavenumbers (cm^{-1}) and symmetry	Experimental wavenumbers (cm^{-1}) in LS state	Assignments[a]
53 E_g		TNH_2 trz	1039 A_{1g}	1042	νNN, δrg
86[b] A_{1g}		TNH_2 trz	1090 E_g	1052	δrg, νC NNH_2, δH C N
103 E_g		TNH_2 trz	1094 A_{1g}	1108	δrg, νC NNH_2, δH C N
147 E_g		LNH_2 trz	1211[b] E_g		δH C N
155 A_{1g}	204	LNH_2 trz	1218 A_{1g}	1202	δH C N
180 E_g		τCN NH_2, LNH_2 trz	1233 A_{1g}		δH C N
211[b] E_g		γNH_2	1265[b] E_g		ρNH_2
217 A_{1g}	246	TNH_2 trz	1266[b] E_g		ρNH_2
224 E_g	257	τCN NH_2, LNH_2 trz	1303 E_g		νC NNH_2, δrg
326[b] E_g		γNH_2	1304 A_{1g}	1374	νC NNH_2
348 A_{1g}	335	δC N NH_2	1375 E_g	1390	νC N, νN NH_2
360[b] E_g		γNH_2, δC N NH_2	1379 A_{1g}	1412	νC N, νN NH_2
411 E_g	443	δC N NH_2	1452 E_g	1482	νC N
435[b] A_{1g}		δC N NH_2	1459 A_{1g}	1485	νC N
535 E_g	634	ωNH_2	1515 A_{1g}	1550	νC N, νC NNH_2, δH C N
544[b] A_{1g}		ωNH_2	1516 E_g		νC N, νC NNH_2, δH C N
650[b] E_g		γrg	1683 E_g	1620	δNH_2
700[b] E_g		γrg	1684 A_{1g}		δNH_2
727 E_g	701	νN NH_2, τrg	3266 E_g	3106	νCH
730 A_{1g}	705	νN NH_2, τrg	3267 A_{1g}	3136	νCH
928[b] E_g		γCH	3328[b] E_g		νCH
942[b] E_g		γCH	3329 A_{1g}	3167	νCH
969 E_g	1010	νNN	3519 E_g	3214	νCH
979 A_{1g}	1020	νNN, δrg	3522 A_{1g}	3277	νNH
1037 E_g	1034	δrg	3678 E_g	3322	νNH

[a] Meaning of symbols: L, librations; T, translations; ν, stretching; δ, deformation or in plane bending; γ, out of plane bending; ω, wagging; τ, torsion; ρ, rocking; rg, ring. [b] The Raman activity calculated for this mode is very low.

In our model system, the complex belongs to the point group symmetry D_{3d} so that a total of 183 vibration modes are expected with the following activities:

$$\Gamma_{\text{Silent}} = 10\,A_{2g} + 11\,A_{1u}$$

$$\Gamma_{\text{Raman}} = 20\,A_{1g} + 30\,E_g$$

$$\Gamma_{\text{IR}} = 20\,A_{2u} + 31\,E_u$$

For the 50 Raman-active vibrations, the induced polarizability tensors α' take the following forms (according to the conventions defined in ref. 41):

$$\alpha'[A_{1g}] = \begin{bmatrix} a & 0 & 0 \\ 0 & a & 0 \\ 0 & 0 & b \end{bmatrix}, \quad \alpha'[E_g(1)] = \begin{bmatrix} c & 0 & d \\ 0 & c & 0 \\ d & 0 & 0 \end{bmatrix}, \quad \alpha'[E_g(2)] = \begin{bmatrix} 0 & c & 0 \\ c & 0 & d \\ 0 & d & 0 \end{bmatrix} \quad (1)$$

Given the form of the polarizability tensors, we can deduce that the $y(xx)\bar{y}$ spectrum should contain A_{1g} and E_g modes, while only A_{1g} modes are expected in the $y(zz)\bar{y}$ spectrum and only E_g modes in the $y(xz)\bar{y}$ spectrum. In order to illustrate the symmetry properties of the Raman active modes, we have schematized in Fig. 5 the external translational Raman active vibrations of the model system. The Raman activity corresponding to a given

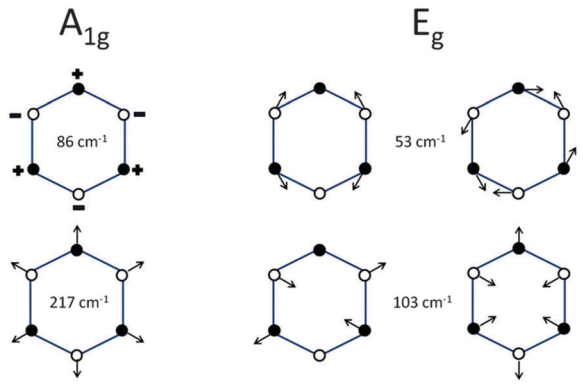

Fig. 5 Schematic representation along the z axis of the translations of the ligands for the Raman active modes A_{1g} and E_g. The circles symbolize the NH_2 trz molecules (filled circles for $z > 0$ and open circles for $z < 0$), the arrows indicate their displacement in the xy plane, the + and − signs indicate their displacement along positive or negative directions of z and the wavenumbers are those calculated by DFT.

polarization geometry is deduced for each calculated normal mode k from the squared values of the components of the induced polarizability tensor α'_k calculated as follows:[42]

$$\alpha'_k = \frac{1}{\sqrt{\mu_k}} \sum_{i\ 1}^{3N} d_k^i \cdot P_k^i \quad (2)$$

where μ_k, d_k^i and P_k^i, are found in the output file of the Gaussian software and represent the reduced mass, the normalized real displacement in Cartesian coordinates (i ranging from 1 to $3N$,

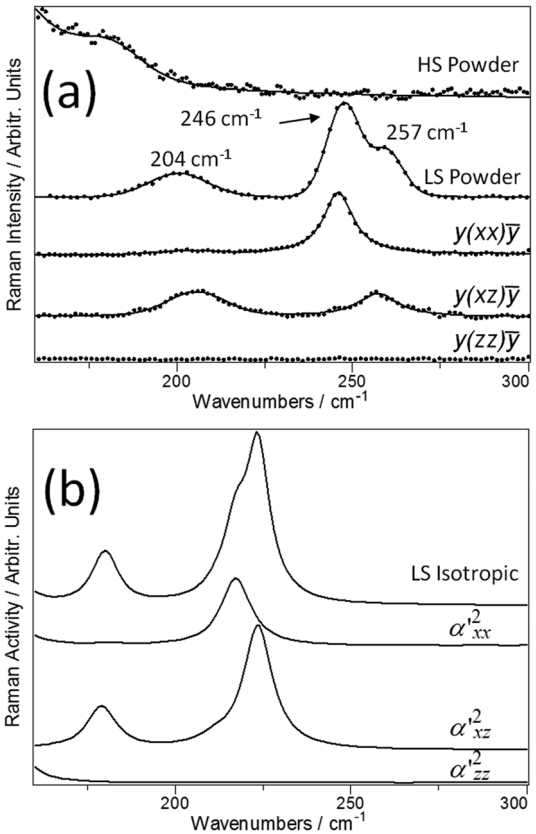

Fig. 6 (a) Experimental Raman spectra (powder sample in the HS and LS states and 3 polarizations for the single crystal in the LS state) and (b) theoretical Raman activities (isotropic and squared components of the Raman tensor) below 300 cm ^{1} for $[Fe(NH_2\ trz)_3](NO_3)_2$.

where N is the number of atoms) and the linear polarizability derivative tensor, respectively. The Raman activity of a normal mode k for an isotropic system is given by $45\bar{\alpha}^2 + 7\gamma^2$ where $\bar{\alpha}$ is the trace and γ^2 the anisotropy of the polarizability tensor α'_k.

At room temperature, for both LS $[Fe(NH_2\text{-}trz)_3](NO_3)_2{\cdot}2H_2O$ single crystals and $[Fe(NH_2\text{-}trz)_3](NO_3)_2{\cdot}H_2O$ powder, 3 modes emerge at 204, 246 and 257 cm^{-1} in the low-wavenumber range between 150 and 300 cm^{-1} (Fig. 6a). The preliminary investigation performed by E. Smit *et al.*[14] on $[Fe(NH_2trz)_3](ClO_4)_2$ in the LS state identified only two bands in this region at 200 and 244 cm^{-1}, the latter being assigned to the Fe-ligand stretching vibration. It should be emphasized that the Raman band at 244 cm^{-1} in ref. 14 is clearly not symmetric and perhaps not sufficiently resolved. Moreover three Raman bands at 200, 239 and 255 cm^{-1} were observed[15] for the $[Fe(NH_2trz)_3](CH_3SO_4)_2$ compound at 273 K. The Raman spectrum recorded in the $y(xz)\bar{y}$ polarization (Fig. 6a) displays 2 bands at 204 and 257 cm^{-1} that belong to E_g representations. From the analysis of the components of the Raman tensors calculated by using the Gaussian package, only two normal modes with significant Raman activities within this spectral window are calculated at 180 and 234 cm^{-1} (see Fig. 6b). These degenerated vibrations with E_g symmetry involve CN–NH_2 torsion vibrations (calculated around 270 cm^{-1} for the free molecule, see Table S1 in ESI†) coupled to libration motions of the ligands. The libration mode calculated at 180 cm^{-1} follows the symmetry rules of the translation mode calculated at 53 cm^{-1} while the libration mode calculated at 234 cm^{-1} follows those of the translation mode calculated at 103 cm^{-1} (see Fig. 5). The Raman spectrum recorded in the $y(xx)\bar{y}$ polarization (Fig. 6a) displays 2 bands, the mode with E_g symmetry calculated at 180 cm^{-1} (Fig. 6b), and a stronger one at 246 cm^{-1}, not observed for the other polarizations, which must consequently be of A_{1g} symmetry. An A_{1g} mode with significant Raman activity is calculated at 217 cm^{-1}, corresponding to in-plane translations of the ligands (breathing mode) as schematized in Fig. 5. This vibration involves not only Fe–ligand stretching but also ligand–Fe–ligand bending. Finally, no Raman bands in Fig. 6a could be observed for the $y(zz)\bar{y}$ polarization, in very good agreement with the theoretical calculations (Fig. 6b).

The spectral region between 950 and 1150 cm^{-1} corresponds to vibrations involving bending and stretching modes of the ligand ring (N–N and C–NNH_2 stretches, NCN, NNC and CNC bends, see the DFT calculations for the isolated molecule in Table S1, ESI†). First of all, a simple comparison between the experimental Raman spectra for different counterions displayed in Fig. 4 allows the identification of the stretching mode of the nitrate ion in the intense Raman band at 1047 cm^{-1}. The accordance between the experimental and theoretical spectra displayed in Fig. 7 is less satisfactory compared to that shown in Fig. 6. Nevertheless, we may adopt the same strategy to assign the observed Raman bands. The experimental spectrum of $[Fe(NH_2\text{-}trz)_3](NO_3)_2{\cdot}2H_2O$ in the $y(xz)\bar{y}$ polarization geometry (Fig. 7a) displays one intense peak at 1010 cm^{-1}, near to the intense E_g peak predicted at 969 cm^{-1} in the same polarization configuration and involving N–N stretching vibrations of the trz ring. Around 1020 cm^{-1} on the experimental spectra, we observe a peak active in the $y(xx)\bar{y}$ polarization (and inactive in the $y(xz)\bar{y}$ polarization) that may be assigned to the A_{1g} mode calculated at 979 cm^{-1}. This vibration also involves N–N stretching as well as deformations of the ring. The band calculated for the isotropic system around 1040 cm^{-1} (Fig. 7b) is the superimposition of two vibrations, an A_{1g} mode calculated at 1037 cm^{-1} (ring deformations) and an E_g mode calculated at 1039 cm^{-1} (N–N stretching and ring deformations). As such an A_{1g} contribution is predicted at $\sim$1037 cm^{-1} in the $y(zz)\bar{y}$ and $y(xx)\bar{y}$ polarization configurations (Fig. 7b), we assign the two experimental peaks at 1034 and 1042 cm^{-1} that are $y(zz)\bar{y}$ and $y(xx)\bar{y}$ polarized to these A_{1g} modes. Similarly, the peak for the isotropic system calculated around 1090 cm^{-1} is the superimposition of an E_g mode calculated at 1090 cm^{-1} (ring deformation) and an A_{1g} mode (N–N stretching and ring deformations) calculated at 1094 cm^{-1}. In this case the $y(xz)\bar{y}$ band at 1052 cm^{-1} is assigned to the E_g vibration calculated at 1090 cm^{-1} and the $y(xx)\bar{y}$ Raman band observed at 1108 cm^{-1} is assigned to the A_{1g} symmetry mode calculated at 1094 cm^{-1}.

The experimental spectra and the calculated Raman activities for the other vibrations in the 1300–1600 cm^{-1} range are displayed in Fig. 8. In this spectral region, C–N, C–NH_2 and C–NNH_2 stretching vibrations are expected (see Table S1, ESI†). Again we

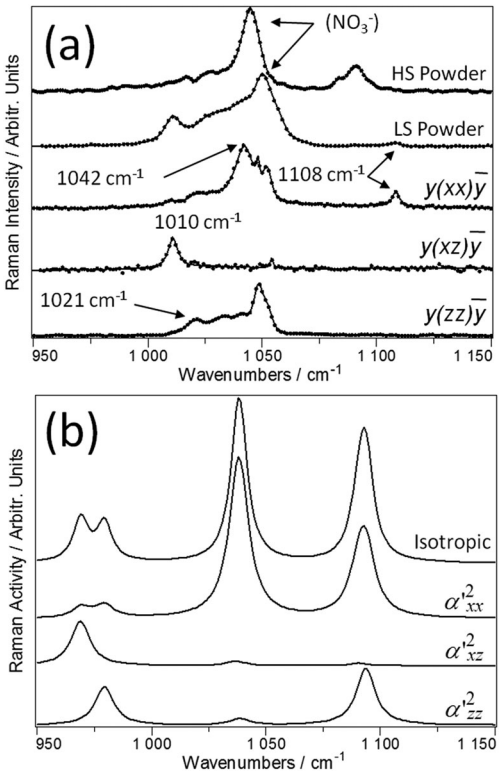

Fig. 7 (a) Experimental Raman spectra (powder sample in the HS and LS states and 3 polarizations for the single crystal in the LS state) and (b) theoretical Raman activities (isotropic and squared components of the Raman tensor) between 950 and 1150 cm ^{1} for $[Fe(NH_2\ trz)_3](NO_3)_2$.

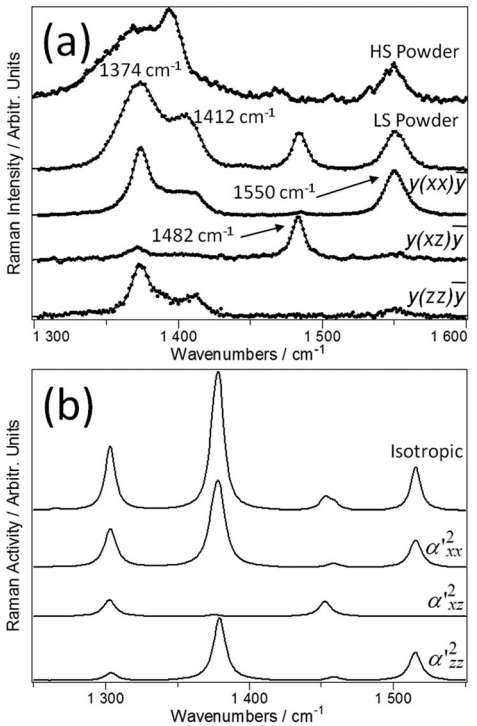

Fig. 8 (a) Experimental Raman spectra (powder sample in the HS and LS states and 3 polarizations for the single crystal in the LS state) and (b) theoretical Raman activities (isotropic and squared components of the Raman tensor) between 1300 and 1550 cm ^{1} for $[Fe(NH_2\ trz)_3](NO_3)_2$.

may propose an assignment following the same method as that described above. For example the peak observed at 1482 cm^{-1} is $y(xz)\bar{y}$ polarized and can be safely assigned to the C–N stretching vibration of E_g symmetry calculated at 1452 cm^{-1}, and the weak peak observed at 1485 cm^{-1} is $y(xx)\bar{y}$ polarized and assigned to the A_{1g} C–N stretching vibration calculated at 1459 cm^{-1}. All the proposed assignments for the Raman active vibrations of the $[Fe(NH_2\text{-}trz)_3](NO_3)_2$ SCO compound in the LS state are summarized in Table 1.

Raman spectra of $[Fe(NH_2\text{-}trz)_3]$ in the HS state

Because of the large electronic rearrangement during the spin crossover process, the iron–ligand bond[40] in the HS state is significantly longer (2.18 Å) than in the LS state (2.01 Å). This rearrangement is reflected in the vibration properties of the complexes, and the vibrational modes most affected by the change in spin state are, *a priori*, the metal–ligand vibrations involving stretching and bending internal coordinates. Raman spectra associated with the LS and HS $[Fe(NH_2\text{-}trz)_3](NO_3)_2$ complex in powder form, within the spectral windows analyzed in detail in the previous section, are shown in Fig. 6a–8a. As previously mentioned by other authors,[14,15] the Raman peaks observed between 150 and 300 cm^{-1} in the LS state (Fig. 6a) can be used as marker bands of the spin transition. Indeed, we have shown that these Raman peaks involve librations and translations of the ligands; thus the characteristic wavenumbers of these vibrations depend strongly on the strength of the Fe–ligand interaction. As a matter of fact, these peaks could not be observed in the HS state at 370 K due to the cut-off of the Notch filter below 150 cm^{-1}, so that we can state that their Raman red shift, due to the LS–HS transition, is of the order of 100 cm^{-1}. In contrast, we do observe in Fig. 7a a blue shift of some peaks on crossing the phase transition. In particular, two Raman bands observed in the LS state at 1010 and 1042 cm^{-1} are significantly upshifted by $\sim$60 cm^{-1} in the HS state, presumably to give rise to the new bands around 1090 cm^{-1}. These modes were assigned to vibrations involving mainly the N–N stretching of the trz rings. Thus, in the HS state, the charge transfer between the iron and nitrogen atoms (N–N bonds) of the ligands is less efficient and the strength of the N–N bonds is consequently larger. Around 1500 cm^{-1} (Fig. 8a) the Raman bands are broadened and red shifted on crossing the phase transition. This is particularly obvious for the peak at 1485 cm^{-1} in the LS state that was assigned to the C–N stretches of the ring. The band at 1550 cm^{-1} assigned to the C–NNH_2 stretching vibration, a functional group that is not in direct interaction with iron, constitutes however an exception since its wavenumber remains almost unaltered.

The hysteresis loop

The hysteresis loop for $[Fe(NH_2\text{-}trz)_3](NO_3)_2$ has already been studied by means of macroscopic and microscopic methods such as reflectivity,[9,11] magnetic susceptibility, DSC calorimetry; Mössbauer spectroscopy and X-ray diffraction.[40] The breadth of the hysteresis loop, the transition temperatures T_{up} measured

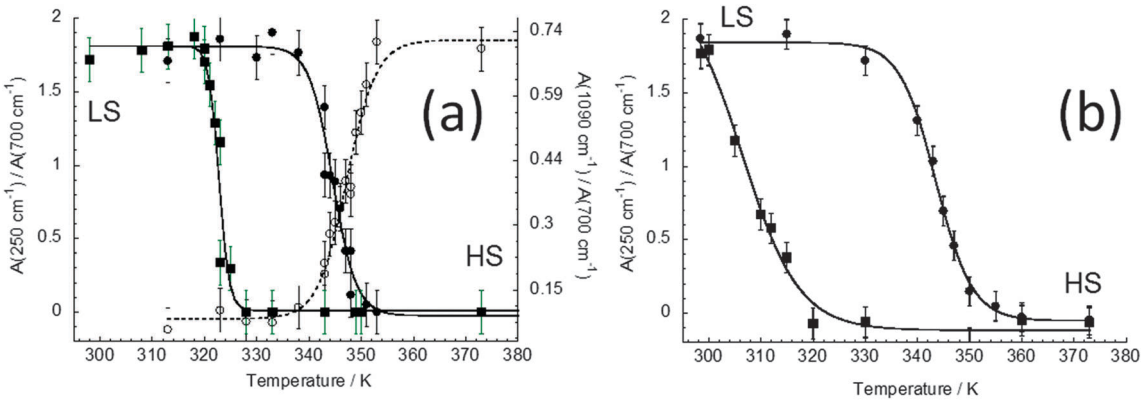

Fig. 9 Hysteresis loops of $[Fe(NH_2\ trz)_3](NO_3)_2$ measured under an atmosphere of dry nitrogen at atmospheric (a) and reduced (b) pressures. Filled symbols correspond to the ratios of the integrated areas of the Raman bands at 250 cm ^{1} and 700 cm ^{1} measured upon heating (circles) and cooling (squares) the sample. The open circles (a) correspond to the ratios of the integrated areas of the Raman band at 1090 cm ^{1} and 700 cm ^{1} measured upon heating the sample (for clarity the values measured upon cooling the sample are not reported).

upon heating and the transition temperatures T_{down} measured upon cooling are found to belong to the 17–38 K, 345–348 K, and 310–328 K ranges, respectively. Vibrational spectroscopy can provide information about the spin transition at a microscopic level using a molecular probe, *i.e.* a specific spin-state-dependent Raman spectral feature. We have seen in the previous section that several Raman bands, in particular the external Fe–ligand vibrations or the N–N stretching modes of the ligand, could be used as markers for characterizing the phase transition. In the following, the spin transition in $[Fe(NH_2\text{-}trz)_3](NO_3)_2$ has been determined by measuring the temperature dependence of the integrated intensities of the Raman bands at 245 and 254 cm^{-1} assigned to the Fe–Ligand external vibrations in the LS state upon cooling or heating the sample between 298 and 390 K, normalized with respect to the N–NH_2 stretching vibration at around 700 cm^{-1}. Indeed, as the N–NH_2 functional group does not interact with the iron atoms, the Raman band assigned to this vibration, well isolated from other peaks, is not significantly broadened or shifted in the HS state. For comparison, we have also used the Raman band at 1090 cm^{-1} in the HS state as a marker for the transition.

It should be emphasized that the transition temperatures measured by means of the various techniques mentioned above converge to the common value $T_{up} \approx 347$ K, but measured values for T_{down} range over ~18 K. Certainly the sample environment may have a significant influence on the thermal equilibrium and consequently on the transition temperatures.

In addition, we found that even low laser fluence could induce the thermal spin transition at room temperature. A precise adjustment of the laser power was therefore necessary to avoid local heating of the sample. A laser power as low as 8 μW and spread over an area of 400 μm^2 was optimal for measuring the transition temperatures confidently. Second, the SCO complex captures water molecules when left in surrounding air at atmospheric pressure and forms the hydrated compound $[Fe(NH_2\text{-}trz)_3](NO_3)_2{\cdot}H_2O$ (see the O–H stretching bands observed around 3500 cm^{-1} on the Raman and IR spectra reported in Fig. 2 for the sample in the LS state). Upon heating, the compound releases water molecules and the transition temperature T_{up} of ~335 K is observed. Because the sample is still immersed in a wet atmosphere, it rehydrates upon cooling and the transition temperature T_{down} is ~325 K. In order to avoid sample hydration, additional experiments were performed by preliminarily heating the sample at 390 K in a dry N_2 atmosphere for 30 min before cooling down to 298 K. The sample was left thermalizing at 298 K before starting a measurement of the hysteresis loop. Whatever the Raman band selected as a marker (Fig. 9a), the measured transition temperatures were $T_{up} = 345 \pm 2$ K and $T_{down} = 325 \pm 2$ K with this dehydrated compound in a dry N_2 atmosphere at the 100 kPa atmospheric pressure. These results are in very good agreement with those obtained by means of reflectivity techniques[9,11] (T_{up} = 347 K and T_{down} = 327 K). Finally, we have measured the hysteresis loop for the sample under reduced pressure (1.3 kPa) and found transition temperatures $T_{up} = 344$ K ± 2 K and $T_{down} = 309 \pm 2$ K (Fig. 9b). The difference between T_{down} transition temperatures inferred from Raman measurements under atmospheric and reduced pressure was as large as 16 K. These results are congruent with the transition temperatures T_{up} = 347 K and T_{down} = 310 K found by means of magnetic susceptibility measurements.[40] They are also coherent with results expected by application of an external pressure[43] on SCO materials. When the pressure increases, the LS state, of smaller volume, is favoured and, conversely, if the pressure is reduced the HS state is stabilized. In the latter case, T_{down} must therefore decrease, as it is observed here at 1.3 kPa or in the magnetic measurements, performed in a SQUID cavity, *i.e.* under a reduced pressure.

These results demonstrate that, at least for $[Fe(NH_2\text{-}trz)_3](NO_3)_2$ compounds, the phase transition may be followed by means of very different techniques probing the structural changes on different scales. The transition temperatures and the hysteresis loops do not depend on the techniques used to perform the measurement, but depend strongly on external parameters such as pressure, humidity or local heating.

Conclusions

In this work, we have shown that water molecules and counter anions present in the structure of the $[Fe(NH_2\text{-}trz)_3](X)_2{\cdot}nH_2O$

SCO complexes had no significant influence on the vibrational properties of the polymer chains. Thus a simplified model of this system could be constructed for DFT calculations. We have proposed in this paper a full vibrational assignment of Raman bands valid for all members of the family of $[Fe(NH_2\text{-}trz)_3](X)_2 \cdot nH_2O$ SCO complexes in the LS state. This assignment was made possible by recording for the first time the polarized Raman spectra of single crystals of $[Fe(NH_2\text{-}trz)_3](NO_3)_2 \cdot 2H_2O$ complexes and by analyzing the DFT-derived Raman activities of the components of the Raman tensors. Several vibrations of the polymer may be used as markers to follow, at a molecular level, the transition phenomenon. The most spectacular changes in the Raman spectra are associated with the metal–ligand vibrations at low wavenumbers below 400 cm^{-1} involving stretching and bending internal coordinates and the trz ring vibrations involving mainly the N–N stretching internal coordinates. We have shown, in agreement with other authors and in particular E. Smit *et al.*,[22] that hysteresis loops obtained from Raman scattering experiments in SCO $[Fe(NH_2\text{-}trz)_3](X)_2$ compounds nicely compare to those determined from very different techniques. Such studies allow the analysis of SCO phenomena using molecular probes. However the sample environment (humidity, pressure, local heating due to the laser power) must be precisely controlled for comparing hysteresis loops obtained by means of Raman spectroscopy to those obtained by means of other techniques.

Acknowledgements

The authors thank the cluster Advanced Materials in Aquitaine (post-doctoral grant to Y. T.), the Conseil Régional d'Aquitaine and Europe (FEDER programme) for funding equipment of the Vibrational Spectroscopy and Imaging (SIV) platform at ISM. Additional support from Conseil Régional d'Aquitaine (PhD grant to A. G.) is also gratefully acknowledged.

Notes and references

1 O. Kahn and C. Jay Martinez, *Science*, 1998, **279**, 44–48.
2 P. Gütlich, Y. Garcia and T. Woike, *Coord. Chem. Rev.*, 2001, **219–221**, 839–879.
3 *Spin Crossover in Transition Metal Compounds I*, ed. P. Gütlich and H. A. Goodwin, 2004, vol. 233.
4 C. Etrillard, V. Faramarzi, J.-F. Dayen, J.-F. Letard and B. Doudin, *Chem. Commun.*, 2011, **47**, 9663–9665.
5 J. Kroeber, J.-P. Audiere, R. Claude, E. Codjovi, O. Kahn, J. G. Haasnoot, F. Groliere, C. Jay and A. Bousseksou, *Chem. Mater.*, 1994, **6**, 1404–1412.
6 J. F. Letard, P. Guionneau and L. Goux-Capes, *Spin Crossover in Transition Metal Compounds III*, Springer, Berlin/Heidelberg, 2004, vol. 235, pp. 221–249.
7 G. Aromí, L. A. Barrios, O. Roubeau and P. Gamez, *Coord. Chem. Rev.*, 2011, **255**, 485–546.
8 A. Bousseksou, G. Molnár, L. Salmon and W. Nicolazzi, *Chem. Soc. Rev.*, 2011, **40**, 3313–3335.
9 G. Galle, J. Degert, C. Mauriac, C. Etrillard, J. F. Letard and E. Freysz, *Chem. Phys. Lett.*, 2010, **500**, 18–22.
10 G. Gallé, C. Etrillard, J. Degert, F. Guillaume, J.-F. Létard and E. Freysz, *Appl. Phys. Lett.*, 2013, **102**, 063302.
11 G. Gallé, D. Deldicque, J. Degert, T. Forestier, J.-F. Létard and E. Freysz, *Appl. Phys. Lett.*, 2010, **96**, 041907.
12 O. Fouche, J. Degert, G. Jonusauskas, N. Daro, J.-F. Letard and E. Freysz, *Phys. Chem. Chem. Phys.*, 2010, **12**, 3044–3052.
13 M. M. Dîrtu, A. Rotaru, D. Gillard, J. Linares, E. Codjovi, B. Tinant and Y. Garcia, *Inorg. Chem.*, 2009, **48**, 7838–7852.
14 E. Smit, B. Manoun and D. de Waal, *J. Raman Spectrosc.*, 2001, **32**, 339–344.
15 S. Rackwitz, J. A. Wolny, K. Muffler, K. Achterhold, R. Rüffer, Y. Garcia, R. Diller and V. Schünemann, *Phys. Chem. Chem. Phys.*, 2012, **14**, 14650–14660.
16 A. Grosjean, N. Daro, B. Kauffmann, A. Kaiba, J.-F. Letard and P. Guionneau, *Chem. Commun.*, 2011, **47**, 12382–12384.
17 A. Grosjean, P. Négrier, P. Bordet, C. Etrillard, D. Mondieig, S. Pechev, E. Lebraud, J.-F. Létard and P. Guionneau, *Eur. J. Inorg. Chem.*, 2013, 796–802.
18 J.-P. Tuchagues, A. Bousseksou, G. Molnár, J. McGarvey and F. Varret, *Spin Crossover in Transition Metal Compounds III*, Springer, Berlin/Heidelberg, 2004, vol. 235, pp. 23–38.
19 Y. A. Tobon, C. Etrillard, O. Nguyen, J.-F. Létard, V. Faramarzi, J.-F. Dayen, B. Doudin, D. M. Bassani and F. Guillaume, *Eur. J. Inorg. Chem.*, 2012, 5837–5842.
20 J. A. Wolny, R. Diller and V. Schünemann, *Eur. J. Inorg. Chem.*, 2012, 2635–2648.
21 J. A. Wolny, H. Paulsen, A. X. Trautwein and V. Schünemann, *Coord. Chem. Rev.*, 2009, **253**, 2423–2431.
22 H. Paulsen and A. X. Trautwein, *Spin Crossover in Transition Metal Compounds III*, Springer, Berlin, Heidelberg, 2004, pp. 197–219.
23 H. Paulsen, V. Schünemann and J. A. Wolny, *Eur. J. Inorg. Chem.*, 2013, 628–641.
24 G. Brehm, M. Reiher and S. Schneider, *J. Phys. Chem. A*, 2002, **106**, 12024–12034.
25 G. Brehm, M. Reiher, B. Le Guennic, M. Leibold, S. Schindler, F. W. Heinemann and S. Schneider, *J. Raman Spectrosc.*, 2006, **37**, 108–122.
26 S. Bonhommeau, N. Bréfuel, V. K. Pálfi, G. Molnár, A. Zwick, L. Salmon, J.-P. Tuchagues, J. S. Costa, J.-F. Létard, H. Paulsen and A. Bousseksou, *Phys. Chem. Chem. Phys.*, 2005, **7**, 2909–2914.
27 K. L. Ronayne, H. Paulsen, A. Höfer, A. C. Dennis, J. A. Wolny, A. I. Chumakov, V. Schünemann, H. Winkler, H. Spiering, A. Bousseksou, P. Gütlich, A. X. Trautwein and J. J. McGarvey, *Phys. Chem. Chem. Phys.*, 2006, **8**, 4685–4693.
28 Y. Garcia, H. Paulsen, V. Schünemann, A. X. Trautwein and J. A. Wolny, *Phys. Chem. Chem. Phys.*, 2007, **9**, 1194–1201.
29 J. A. Wolny, S. Rackwitz, K. Achterhold, Y. Garcia, K. Muffler, A. D. Naik and V. Schünemann, *Phys. Chem. Chem. Phys.*, 2010, **12**, 14782–14788.
30 G. Lemercier, N. Bréfuel, S. Shova, J. A. Wolny, F. Dahan, M. Verelst, H. Paulsen, A. X. Trautwein and J.-P. Tuchagues, *Chem.–Eur. J.*, 2006, **12**, 7421–7432.

31 Y. Chumakov, G. S. Matouzenko, S. A. Borshch and A. Postnikov, *Polyhedron*, 2009, **28**, 1955–1957.
32 L. G. Lavrenova, V. N. Ikorskii, V. A. Varnek, I. M. Oglezneva and S. V. Larionov, *Koord. Khim.*, 1986, **12**, 207–215.
33 V. G. Bessergenev, G. A. Berezovskii, L. G. Lavrenova and S. V. Larionov, *Russ. J. Phys. Chem.*, 1996, **71**, 714–718.
34 O. Kahn, E. Codjovi, Y. Garcia, P. J. van Koningsbruggen, R. Lapouyade and L. Sommier, in *Molecule-Based Magnetic Materials*, ed. M. M. Turnbull, T. Sugimoto and L. K. Thompson, American Chemical Society, Washington, DC, 1996, vol. 644, pp. 298–310.
35 M. J. Frisch, G. W. Trucks, H. B. Schlegel, G. E. Scuseria, M. A. Robb, J. R. Cheeseman, G. Scalmani, V. Barone, B. Mennucci, G. A. Petersson, H. Nakatsuji, M. Caricato, X. Li, H. P. Hratchian, A. F. Izmaylov, J. Bloino, G. Zheng, J. L. Sonnenberg, M. Hada, M. Ehara, K. Toyota, R. Fukuda, J. Hasegawa, M. Ishida, T. Nakajima, Y. Honda, O. Kitao, H. Nakai, T. Vreven, J. A. Montgomery Jr., J. E. Peralta, F. Ogliaro, M. Bearpark, J. J. Heyd, E. Brothers, K. N. Kudin, V. N. Staroverov, R. Kobayashi, J. Normand, K. Raghavachari, A. Rendell, J. C. Burant, S. S. Iyengar, J. Tomasi, M. Cossi, N. Rega, J. M. Millam, M. Klene, J. E. Knox, J. B. Cross, V. Bakken, C. Adamo, J. Jaramillo, R. Gomperts, R. E. Stratmann, O. Yazyev, A. J. Austin, R. Cammi, C. Pomelli, J. W. Ochterski, R. L. Martin, K. Morokuma, V. G. Zakrzewski, G. A. Voth, P. Salvador, J. J. Dannenberg, S. Dapprich, A. D. Daniels, O. Farkas, J. B. Foresman, J. V. Ortiz, J. Cioslowski and D. J. Fox, *Gaussian 09, Revision A.2*, Gaussian Inc., Wallingford, CT, 2009.
36 W. R. Wadt and P. J. Hay, *J. Chem. Phys.*, 1985, **82**, 284–298.
37 P. J. Hay and W. R. Wadt, *J. Chem. Phys.*, 1985, **82**, 270–283.
38 M. H. Palmer and D. Christen, *J. Mol. Struct.*, 2004, **705**, 177–187.
39 I. Matulková, I. Němec, K. Teubner, P. Němec and Z. Mička, *J. Mol. Struct.*, 2008, **873**, 46–60.
40 M. M. Dîrtu, C. Neuhausen, A. D. Naik, A. Rotaru, L. Spinu and Y. Garcia, *Inorg. Chem.*, 2010, **49**, 5723–5736.
41 J. Brandmüller, R. Claus and L. Merten, *Light Scattering by Phonon-Polaritons*, Springer-Verlag, Berlin, Heidelberg, New York, 1975, vol. 75.
42 L. Ru and P. G. Etchegoin, *Principles of Surface-Enhanced Raman Spectroscopy*, Elsevier, Amsterdam, 2009, pp. 465–490.
43 P. Guionneau and E. Collet, in *Spin-Crossover Materials*, ed. L. a. Halcrow, John Wiley & Sons Ltd, 2013, pp. 507–526.